

Comparative study of serum protein binding to three different carbon-based nanomaterials

Maja Sopotnik ^a, Adrijana Leonardi ^b, Igor Križaj ^{b,c,d}, Peter Dušak ^e, Darko Makovec ^e, Tina Mesarič ^a, Nataša Poklar Ulrih ^{d,f}, Ita Junkar ^g, Kristina Sepčič ^{a*}, Damjana Drobne ^{a,*}

^a University of Ljubljana, Biotechnical Faculty, Department of Biology, Večna pot 111, SI-1000 Ljubljana, Slovenia

^b Department of Molecular and Biomedical Sciences, Jožef Stefan Institute, Jamova 39, SI-1000 Ljubljana, Slovenia

^c Department of Chemistry and Biochemistry, Faculty of Chemistry and Chemical Technology, University of Ljubljana, Aškerčeva 5, SI-1000 Ljubljana, Slovenia

^d Centre of Excellence for Integrated Approaches in Chemistry and Biology of Proteins, Jamova 39, SI-1000 Ljubljana, Slovenia

^e Department for Materials Synthesis, Jožef Stefan Institute, Jamova 39, SI-1000 Ljubljana, Slovenia

^f University of Ljubljana, Biotechnical Faculty, Department of Food Science and Technology, Jamnikarjeva 101, SI-1000 Ljubljana, Slovenia

^g Department of Surface Engineering and Optoelectronics, Jožef Stefan Institute, Jamova 39, Ljubljana SI-1000, Slovenia

* Corresponding authors. Tel: +386 1 3203 419. E-mail: kristina.sepcic@bf.uni-lj.si (Kristina Sepčič). Tel: +386 1 3203 375. E-mail: damjana.drobne@bf.uni-lj.si (Damjana Drobne).

Abstract

Nanomaterials (NM) that enter a biological environment are immediately covered by a layer of proteins, which form a protein corona that governs further interactions of NM within the organism. In this study, we investigated the bovine serum albumin corona and the human serum protein corona, formed on three different carbon-based NM: carbon black, multi-walled carbon nanotubes, and graphene oxide. The serum protein corona of all three studied NM was found to be enriched with complement factors and apolipoproteins. In addition, by measuring the enzymatic activity of the serum butyrylcholinesterase, we have shown that also less abundant proteins could be included in and affected by the corona formation. The studied NM show NM-specific affinities towards albumin binding, both in the pure bovine serum albumin solution or in the human serum. Interestingly, graphene oxide has the lowest affinity towards albumin, but it shows the highest sorptive capacity for other serum proteins, including those present in small amounts.

1. Introduction

In recent years, nanomaterials (NM) have been developed as useful tools for application in medicine and biology [1–4]. Upon contact with the biological environment, different NM are immediately coated by a layer of proteins that form the so-called protein corona [5]. This protein layer is consequently responsible for interactions inside the organism, such as biodistribution, biocompatibility, and the destiny of the NM [6]. The protein corona is a dynamic formation. As the NM passes from one biological fluid to another, some proteins may detach from the NM and new proteins get adsorbed [7]. It is well known from the literature that unspecific and random binding of blood proteins to NM determines their interactions with cells [8–11]. Therefore the structure of the protein corona is of vital importance in understanding the interaction of NM with biological systems [2,12] and it also plays a key role in targeted drug delivery.

Different NM were shown to bind different proteins, and the intensity of this binding depends both on the properties of the NM and the proteins [13–18]. Regarding the NM surface charge, adsorption potential, particle size and shape are among the main properties that can influence a specific binding of proteins [5, 13, 15, 19–25]. Regarding proteins their attachment to NM surface depends on protein shape [14], size [26–28], charge [15,20], and also on protein concentration [21,29,30]. In order for NM to be used as drug carriers, opsonisation, e.g. the process of removal of NM from the systemic circulation, and their phagocytosis by hepatic Kupffer cells should be minimized, otherwise the drug-loaded NM will be cleared by the organism and will not release the drug at the desired site [26,31,32]. Proteins acting as opsonins are preferentially complement factors, immunoglobulins and fibronectin. In addition, the attachment of apolipoproteins that facilitate the translocation of NM through the blood brain barrier, should be considered when using NM in medical applications [33,34].

Carbon-based NM are considered to be among the most sorptive of the manufactured NM, and have been known to adsorb both small molecules [35] and larger proteins [23,36]. For example, the binding of proteins to carbon nanotubes (CNT), namely single walled CNT (SWCNT), occurs *via* hydrophobic amino acid residues, and the intensity of this binding correlates with the number of the contact amino acid residues, the number of all hydrophobic residues, the contact area and the size of the protein [37]. It has been shown that CNT adsorb serum albumin, apolipoproteins, fibrinogen, and complement component C1q, which activates

the human complement *via* a classical pathway [38]. SWCNT coated with bovine serum albumin (BSA) can also activate the complement system *via* C1q recognition, while the PEGylated SWCNT activate the complement *via* a lecithin pathway [39]. In addition, the biodistribution of PEGylated CNT in mice was found to be influenced mostly by the presence or absence of apolipoprotein H in the protein corona [17], while the pre-coating of SWCNT with BSA can facilitate the uptake of SWCNT into cells [40]. It has been also shown that the mechanism of the cell uptake of the BSA-coated graphene oxide (GO) sheets was dependent on the flake size [41].

The proteins adsorbed on the NM surface can lose their native conformation [42]. The degree of alterations in the protein secondary and tertiary structure depends both on the protein structure [43–46], as well as on the properties of the NM, such as particle size, surface curvature and surface charge [13,47–51]. Consequently, alterations in the protein secondary and tertiary structures can result in loss of protein function [44,47,49,52,53]. In line with this, previous *in vitro* studies have shown that physiologically important enzymes acetylcholinesterase (AChE) and butyrylcholinesterase (BChE) readily adsorb to a carbon-based NM surface, and that this adsorption is correlated to the loss of enzyme activity [54–56]. The possibility to measure activity of AChE and BChE after exposure to NM makes these two enzymes perfect candidates for model biosensor systems in studying the biological reactivity of NM. AChE is a key enzyme in the nervous system, which enables the transmission of the signals in cholinergic synapses through a degradation of the neurotransmitter acetylcholine [57]. In addition, AChE has recently been identified also in a number of non-neuronal tissues from mammalian species, acting as a local cellular signalling molecule [58]. BChE is found in the blood plasma of vertebrates [59], it is less specific for different substrates than AChE, and can degrade different exogenous toxic compounds [57]. It is assumed that BChE can serve as a backup to AChE, especially when the AChE activity is compromised or absent in supporting and regulating the cholinergic transmission [60].

The aim of our work was to test the affinity of three carbon-based NM for the most abundant serum protein, albumin, and their affinity towards a mixture of serum proteins. It is expected that the most abundant proteins will be also most strongly represented in the protein corona, but in this regard there are differences among NM documented in the literature [19–21,23,38]. We hypothesized that if a NM strongly binds the serum albumin, the other serum proteins will be excluded from the corona formation, or will be present in much lesser amounts. To prove this hypothesis, we first incubated carbon black (CB), multi-walled CNT (MWCNT) or GO in

a suspension of bovine serum albumin (BSA) and tested the intensity of BSA binding to these three different NM. In the second part of the study, we incubated these three NM in the human serum. We assumed that NM which are more prone to bind albumin in a pure suspension will retain this high affinity towards albumin also in a complex mixture when compared with other tested NM. In addition, we have tested also the involvement of a low-abundant serum protein in the corona formation by measuring the activity of the intrinsic serum BChE. It was expected that, if BChE is involved in the protein corona formation, its activity will be inhibited due to the conformational changes after adsorption. We discuss the importance of knowing the composition of the NM protein corona with special emphasis on those types of proteins which are responsible for blood circulation time or blood brain barrier translocation, as well as the potential of NM to adsorb less abundant but physiologically also very relevant serum proteins.

2. Experimental

2.1. Materials

Carbon black nanopowder PL-CB13 with > 99% purity was obtained from PlasmaChem GmbH (Berlin, Germany). According to the supplier, the average primary particle size was 13 nm, and the specific surface area was $570 \pm 20 \text{ m}^2/\text{g}$. Data on our own characterisation are provided in the Section 3.1. Graphene oxide was purchased from Graphene Supermarket (USA) as dry platelets composed of 79 % carbon and 21 % oxygen. According to the producer, the flake size was 0.5-5.0 μm with GO layers of $1.1 \pm 0.2 \text{ nm}$ thickness, while at least 80 % of GO was single-layered. Multi-walled carbon nanotubes were obtained from Nanocyl (Belgium) within the EU FP7 large-scale integrating project NanoValid. According to the manufacturer, MWCNT were 35-50 nm wide. AChE from the electric eel (*Electrophorus electricus*) type VI-S, BChE from equine serum and albumin from bovine serum, fraction V, $\geq 96 \%$ (GE) were purchased from Sigma-Aldrich Co. (USA). AB-human serum from Invitrogen™ was purchased from Life Technologies (Thermo Fisher Scientific Inc., USA). Acetonitrile (Fisher Scientific Ltd., Loughborough, UK) and formic acid (Acros Organics, Geel, Belgium) were of HPLC gradient grade or higher. Deionized water was purified using a Milli-Q system (Millipore Corp., Billerica, MA, USA). All other reagents used for the enzyme assays were obtained from Sigma-Aldrich Co. and were of the highest purification grade available.

2.2. *Methods*

2.2.1. *Preparation of pristine and BSA-coated NM suspensions*

The stock suspensions of pristine NM were prepared in MilliQ water at concentrations of 1 and 2 mg/mL for the assay of isolated AChE and BChE activity, and at concentrations of 2 and 10 mg/mL for the assay of intrinsic human serum BChE activity. These suspensions were sonicated (Sonics Vibra Cell, Newtown, USA) for 1 hour at 39 % amplitude and for 15 seconds on / 15 seconds off cycle, by cooling the suspensions in an ice bath. For experiments with the BSA-coated NM, 1 mg/mL stock suspensions of CB or MWCNT, or 2 mg/mL stock suspension of GO were mixed with equal volume (750 μ L) of different concentrations of BSA in MilliQ water, and incubated for 1 hour at 37 °C with constant shaking at 180 rpm. Following incubation, the mixtures were immediately centrifuged at 15,000 g for 10 minutes, and the supernatant was discarded. The sediment was resuspended in 1500 μ L MilliQ water and used for the AChE or BChE activity assay. For gel electrophoresis, the stock suspensions of pristine NM (2 mg/mL) were prepared in an erythrocyte buffer (140 mM NaCl, 20 mM TRIS, pH 7.4) as described above.

2.2.2. *Characterization of NM*

The pristine NM suspensions were observed by transmission electron microscopy (TEM). Materials were deposited on a perforated, transparent carbon foil supported by copper grid by drying their water suspensions. The TEM analyses were performed with a field-emission electron-source JEOL 2010F microscope operated at 200 kV. The microscope is equipped with energy-dispersive X-ray (EDX) spectrometer Oxford Instruments EDXS-ISIS300. Morphological features of GO were additionally analysed by atomic force microscopy (AFM, Solver PRO, NT-MDT, Russia) in tapping mode in air. One μ l of GO suspension in MilliQ water (50 μ g/mL) was dropped on the perfectly flat silica wafer and the samples were left to dry in air. Samples were scanned with the standard Si cantilever with a force constant of 22 N/m and at a resonance frequency of 325 kHz (tip radius was 10 nm and the tip length was 95 μ m) and with the scan rate set at 1.3 Hz.

The size distribution of CB (47.6 or 4.76 μ g/mL) suspension in MilliQ water or CB (4.76 μ g/mL) suspended in the mixture of Ellman's reagent and 100 mM phosphate buffer, pH 8.0, was analyzed by dynamic light scattering (DLS). For the DLS analysis, Fritsch Analisette 12

DynaSizer was used. The ζ -potential of the NM suspensions was measured using a Brookhaven Instruments Corp., ZetaPALS.

2.2.3. *Cholinesterase activity assay*

The adsorption of AChE and BChE on different NM and the inhibition of these enzymes by NM were assayed by Ellman's method adapted for microtiter plates as described in Mesarič et al. [56]. Briefly, for inhibition measurements, 10 μ L of NM suspensions (0.01-2 mg/mL) were combined with 50 μ L of AChE or BChE solution (0.06 and 0.01 U/mL, respectively) in 100 mM phosphate buffer pH 8.0. After a 10-minute incubation, 100 μ L of Ellman's reagent and 50 μ L of the substrate acetylthiocholine chloride (2 mM) were added and the enzyme reaction was allowed to proceed for 5 minutes, after which the tubes were centrifuged for 5 minutes at 14,500 g. From each tube, 210 μ L of the supernatant was pipetted onto a microtiter plate, and the absorbance of the supernatant at 405 nm was measured 20 minutes after the addition of the substrate to the reaction mixture, using the microplate multimode detector Anthos Zenyth 3100 (Anthos Labtec Instruments GmbH, Austria). To determine the adsorption rate of the enzymes onto the NM, the procedure was modified so that during the 10-minute NM-enzyme incubation all mixtures were centrifuged for 5 minutes at 14,500 g in order to remove the NM-adsorbed enzyme, and the supernatants (60 μ L) containing the non-adsorbed enzyme were pipetted onto the microtiter plate. Immediately, 100 μ L of Ellman's reagent and 50 μ L of 2 mM substrate were added to each well. The absorbance was read at 405 nm exactly 20 minutes after the addition of the substrate to the reaction mixture.

2.2.4. *Circular dichroism-spectroscopic studies of acetylcholinesterase-NM interactions*

The circular dichroism (CD) spectra of electric eel AChE (0.5 mg/mL) in 100 mM phosphate buffer, pH 8.0 at 25 °C were obtained using an AVIV 62DS spectrophotometer (Lakewood, NJ, USA). Spectra were recorded in a 1 mm path length quartz cell for the far UV (198-250 nm) (Starna, Atascadero, CA, USA). CD measurements were performed with a step size of 1.0 nm, a spot width of 1.5 nm, and an average time of 2 seconds. The CD spectra of appropriate NM in 100 mM phosphate buffer pH 8.0 were recorded and subtracted from the protein spectra. The enzyme was titrated with NM (0-286 μ g/mL) directly in the cuvette, therefore the spectra were multiplied by a dilution factor. For all spectra, an average of 3 experimental repeats was calculated. The mean residue ellipticity, $[\Theta]_{\lambda}$, was calculated by using the relation

$$[\Theta]_{\lambda} = \frac{M_o \Theta_{\lambda}}{100 \cdot c \cdot l} \quad [61]$$

in which M_o is the mean residue molar mass ($129.9 \text{ g}\cdot\text{mol}^{-1}$ for electric eel AChE), Θ_{λ} is the measured ellipticity in degrees, c is the concentration in g/ml , and l is the path length in decimeters. $[\Theta]_{\lambda}$ was expressed in $\text{deg cm}^2 \text{ dmol}^{-1}$. The secondary structure content was calculated from the far-UV CD spectra using the CONTIN software package [61].

2.2.5. Investigation of the interaction of serum proteins and NM

2.2.5.1. Human serum butyrylcholinesterase activity assay

The human serum BChE activity assay was performed as described in 2.2.3., with $50 \mu\text{L}$ of 0.4 % (v/v) human serum in 100 mM phosphate buffer pH 8.0 used as a source of enzyme (total protein concentration of $0.392 \text{ mg}/\text{mL}$). The final concentration of serum proteins in the reaction mixture was $0.093 \text{ mg}/\text{mL}$. Stock suspensions (2 or $10 \text{ mg}/\text{mL}$) of NM were used and diluted as described in 2.2.3.

2.2.5.2. Gel electrophoresis

In order to investigate the adsorption of serum proteins to NM, $25 \mu\text{L}$ of NM stock suspensions ($2 \text{ mg}/\text{mL}$) were combined with $75 \mu\text{L}$ of human serum (100, 50, 20, 10, or 2 % v/v in erythrocyte buffer). Mixtures were vortexed and incubated for 1 hour at $37 \text{ }^{\circ}\text{C}$ and by constant shaking (550 rpm). Immediately, after a 15-minute centrifugation at $20,238 \text{ g}$, the supernatants were pipetted into fresh Eppendorf tubes. The supernatants of 100 %, 50 %, 20 % and 10 % NM-serum mixtures were diluted 50-, 20-, 10- and 5-folds, respectively, with erythrocyte buffer. The protein concentration in the diluted supernatants was measured using the BCA Protein Assay Kit (Thermo Fisher Scientific Inc., USA). The absorbance of the particle-free and serum-free control was subtracted from the samples and total protein concentration was calculated relative to the BSA standard. Sediments were washed 3 times by adding $100 \mu\text{L}$ MilliQ water, transferred into new Eppendorf tubes, and centrifuged for 15 minutes at $20,238 \text{ g}$, after that the supernatants were discarded. Finally, the sediments were re-suspended in $20 \mu\text{L}$ erythrocyte buffer and combined with $5 \mu\text{L}$ of 5x SDS buffer (10 % SDS, 25 % glycerol, 0.5 % Coomassie Brilliant Blue (m/V), 300 Mm TRIS-HCl, 0.05 M DTT, pH 8.8), sonicated for 5 minutes in an ultrasonic bath (400 W, 30 kHz; Sonis 4GT, Iskra Pio d.o.o., Slovenia), heated at $95 \text{ }^{\circ}\text{C}$ for 5 minutes and centrifuged for 5 minutes at $20,238 \text{ g}$

in order to separate the proteins from the NM. Aliquots of 14 μ L were loaded on 10 % sodium dodecyl sulphate (SDS)-polyacrylamide gel in SDS running buffer (10 g SDS, 30.3 g TRIS, 144 g glycine, 10 L dH₂O) and resolved at 195 V. After electrophoresis, the gels were stained overnight at room temperature using the Coomassie staining solution (2,5 g Coomassie Brilliant Blue, 500 mL dH₂O, 400 mL MeOH, 100 mL acetic acid), and de-stained in methanol:acetic acid:water at 3:2:15 (v:v:v).

For the mass spectrometry (MS) analysis of the NM protein corona, 10 μL of GO, and 25 μL of MWCNT or CB were mixed with respectively 90 or 75 μL of human serum (50 %, 20 % and 10 % v/v in erythrocyte buffer and further prepared as described above. Aliquots of 20 μL were loaded on 10 % NuPAGE Bis-Tris Gel (Life Technologies, Thermo Fisher Scientific Inc., USA) in MOPS-SDS running buffer (50 mM MOPS, 50 mM TRIS, 0.1% SDS, 1 mM EDTA, pH 7.7) and resolved at 195 V. After the electrophoresis the gels were stained with PageBlue Protein Staining Solution (Thermo Fisher Scientific Inc., USA) for 1 hour and de-stained overnight in MilliQ water.

2.2.5.3. *Mass spectrometry*

In order to analyze the protein composition of the carbon-based NM corona, selected protein spots, namely the ones that were more pronounced at low serum concentrations and thus representing the proteins with the highest affinity towards the NM, but also the more prominent protein spots representing the most abundant proteins, were manually excised from the SDS-PAGE gel for the MS analysis. Each protein spot was cut into small pieces and de-stained with 25 mM NH_4HCO_3 /50 % acetonitrile (ACN), then dehydrated in 100 % ACN, and vacuum-dried. Cysteins were reduced and alkylated using 10 mM DTT and 55 mM iodoacetamide, then the gels were washed with 25 mM NH_4HCO_3 and 100 % ACN, and vacuum-dried. The proteins were digested in gel using a MS grade modified trypsin (Promega) in 25 mM NH_4HCO_3 at 37 °C overnight. The resulting peptides were extracted with 50 % (v/v) ACN/5 % (v/v) formic acid, concentrated in vacuum to 15 μL , and stored at -20 °C. Extracts were purified on StageTips C18 (Thermo Fisher Scientific Inc., USA) according to the manufacturer's instructions and analyzed using an electrospray ionization (ESI) ion trap-MS (MSD Trap XCT Plus, Agilent, USA) as described in Leonardi et al. [62] Liquid chromatography-ESI-MS spectral data, obtained as Mascot generic files (mgf), were searched in the protein databases (SwissProt for proteins with constant domains and NCBI nr for antibodies) using the Mascot search engine. The identified protein database entries are presented in descending order in the search results, based on their scores. A protein that receives more matching MS/MS scans in the search receives a higher overall score and is ranked higher in the search results. The top listed match is often the most abundant protein in the sample.¹

¹ <http://sbs.umkc.edu/documents/MASCOTprobabilitiesNEW.pdf>

3. Results

3.1. Characteristics of nanomaterials

The tested NM differ both structurally and chemically. CB and MWCNT are hydrophobic, pure carbon-based NM that exist respectively in the form of amorphous carbon or rolled-up graphene sheets. On the other hand, GO is a single planar layer of carbon atoms that is arranged into a honeycomb-like lattice, and has a hydrophilic character due to its oxygen-containing (e.g., epoxy, carboxyl, hydroxyl) functional groups.

The TEM analysis of CB revealed aggregates of amorphous, globular NM with a primary size of approximately 20 nm (**Fig. 1A**), while the MWCNT analysis showed bundles of multi-walled CNT with internal diameter of 1.8-10 nm and external diameter of 5.7-15 nm, with some graphite impurities (**Fig. 1B**). The energy-dispersive X-ray spectroscopy (EDXS) analysis of MWCNT showed the mean peak of carbon, together with a substantial peak of oxygen and smaller peaks of Al, Si and Fe (data not shown). After the drying of the GO suspension on the TEM specimen support, the material was deposited in a form of platelet particles, which represent compact, layered aggregates of graphene oxide molecules. At the thin parts of the GO aggregates the layers are frequently wrinkled, giving an uneven contrast of the TEM image (**Fig. 1C**). The EDXS analysis of GO showed that besides carbon and oxygen, small amounts of K and S are present as the impurities (data not shown). Additionally, height and 3D images of the GO surface obtained by AFM (**Supporting Fig. 1**) clearly show the presence and the distribution of GO on the perfectly flat surface of silica wafer. The height of GO evaluated from AFM analysis is about 70 to 120 nm and the length is about 15 to 30 nm. From phase image we can obtain information about viscoelastic properties of the surface and GO can be clearly observed as the darker parts correspond to GO particles on the surface.

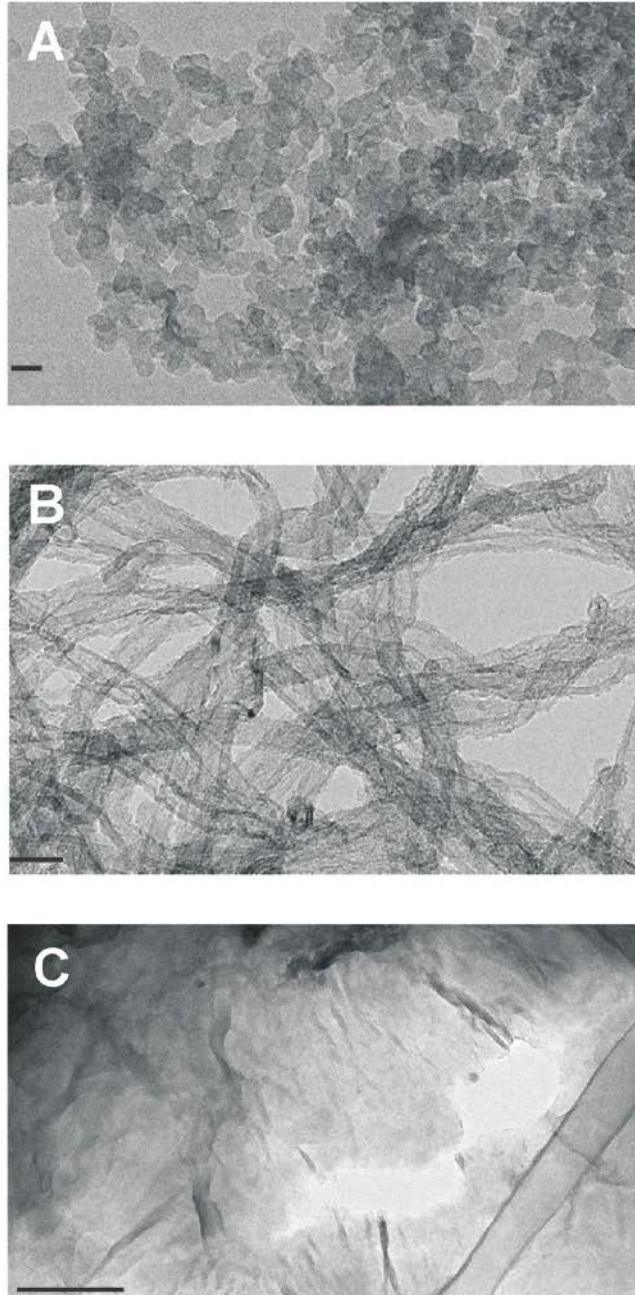


Fig. 1. Transmission electron microscopy images of dried aqueous suspensions of carbon black (A), multi-walled carbon nanotubes (B) and graphene oxide (C). Bars: CB, MWCNT: 20 nm, GO: 500 nm.

The hydrodynamic diameter of CB (47.6 $\mu\text{g/mL}$) suspended in MilliQ ranged between 50 nm and 190 nm, most of the particles having a hydrodynamic diameter between 50 nm and 65 nm (**Fig. 2A**). Similar results were obtained with a more diluted suspension (4.76 $\mu\text{g/mL}$), with some aggregates reaching up to 500 nm (**Fig. 2B**). However, in the mixture of Ellman's

reagent and 100 mM phosphate buffer, the agglomeration of NM occurred, and the hydrodynamic diameter of CB agglomerates ranged between 800 nm and 9400 nm, most of them having a hydrodynamic diameter of 800 nm (**Fig. 2C**). The DLS analysis of the GO and MWCNT suspensions was not possible due to their anisotropic shape. The hydrodynamic diameters of the BSA-coated NM could not be measured because of the agglomeration and sedimentation of the BSA-NM complexes. Similarly, the hydrodynamic diameters of the NM in serum could not be measured due to agglomeration as well.

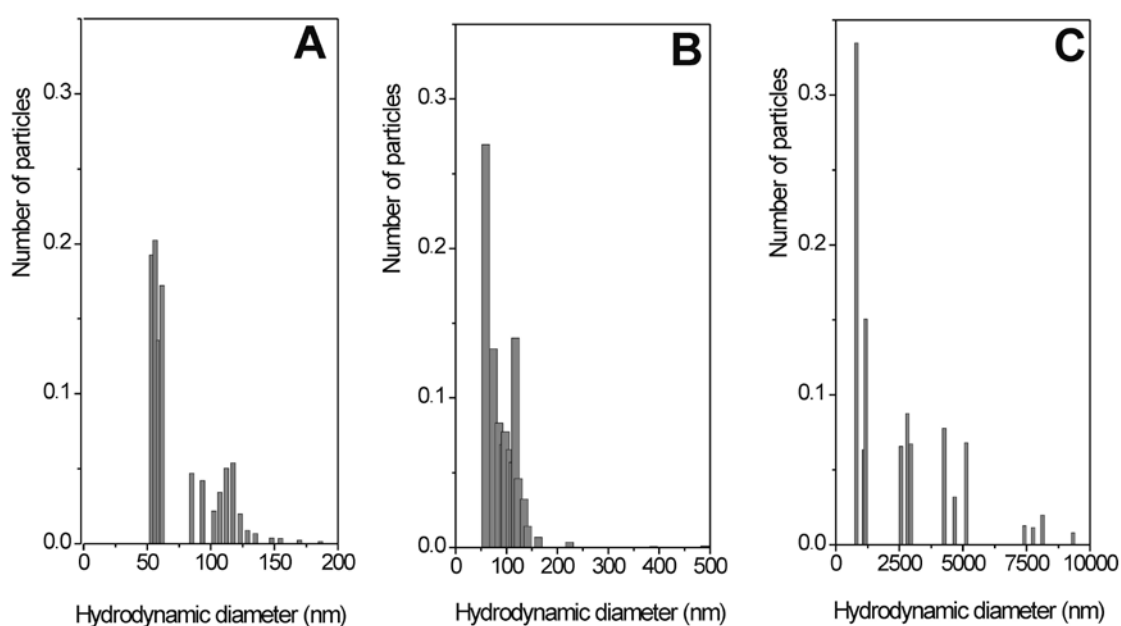


Fig. 2. Number-weighted distributions of hydrodynamic particle size in the suspension containing 47.6 (A) or 4.76 µg/mL (B, C) of the CB suspended in MilliQ (A, B), or in the mixture of Ellman's reagent and 100 mM phosphate buffer (C), measured using DLS.

The zeta potential of CB, MWCNT and GO suspensions in MilliQ was -32 mV, -21 mV and -35 mV, respectively. The zeta potential of CB, MWCNT and GO suspensions in the mixture of Ellman's reagent and 100 mM phosphate buffer was -34 mV, -39 mV and -32 mV, respectively, while the zeta potential of CB, MWCNT and GO in erythrocyte buffer was -12 mV, -10 mV and -21 mV, respectively.

3.2. Effect of BSA-coating of nanomaterials on their ability to adsorb and inhibit cholinesterases

3.2.1. The interaction of uncoated nanomaterials with cholinesterases

The uncoated CB was found to be highly sorptive for both AChE from *Electrophorus electricus*, and BChE from equine serum, causing a 20 % adsorption (EC_{20}) at the respective concentrations of 0.1 and 0.18 $\mu\text{g/mL}$ (**Fig. 3**). The sorptive ability of the uncoated GO for AChE was slightly lower (EC_{20} at 0.3 $\mu\text{g/mL}$), but on the other hand very prominent for BChE ($EC_{20} < 0.048 \mu\text{g/mL}$) (**Fig. 4**). The adsorption rate of AChE and BChE to the uncoated CNT was comparable (EC_{20} around 2 $\mu\text{g/mL}$, **Fig. 5**), however considerably lower when compared to the adsorption to CB and GO. The rate of adsorption of both enzymes to the uncoated CB or MWCNT was close to the rate of the enzyme inhibition by these NM (**Figs. 3 and 5**), suggesting that this inhibition is predominantly caused by adsorption. On the contrary, the adsorption rates to the uncoated GO were higher than the inhibition rates (**Fig. 4**). For example, 5 and 12-folds more of GO was necessary to obtain the 20 % inhibition of AChE and BChE, compared to the amount necessary for the 20 % adsorption. These observations show that a fraction of the GO-adsorbed AChE or BChE still retains its enzymatic activity.

3.2.2. The impact of BSA-corona on the interaction of nanomaterials with cholinesterases

After coating the NM with BSA, the adsorption of both AChE and BChE on all three NM decreased, consequently reducing the inhibition (**Figs. 3-5**). Different amounts of BSA were needed to reduce the interaction of cholinesterases with different NM. In the case of CB, the adsorption to and the inhibition of both enzymes was nearly abolished when the NM was coated with 0.125 mg/mL BSA. In other words, approximately 500-fold more BSA-coated CB was needed to induce the same degree of adsorption and inhibition of cholinesterases in comparison to the uncoated CB. A similar effect was observed with MWCNT coated with 0.15 mg/mL BSA. The protective effect of BSA was considerably less pronounced with GO, where comparable decreases in the rate of adsorption/inhibition appeared only at very high BSA concentrations (4 mg/mL).

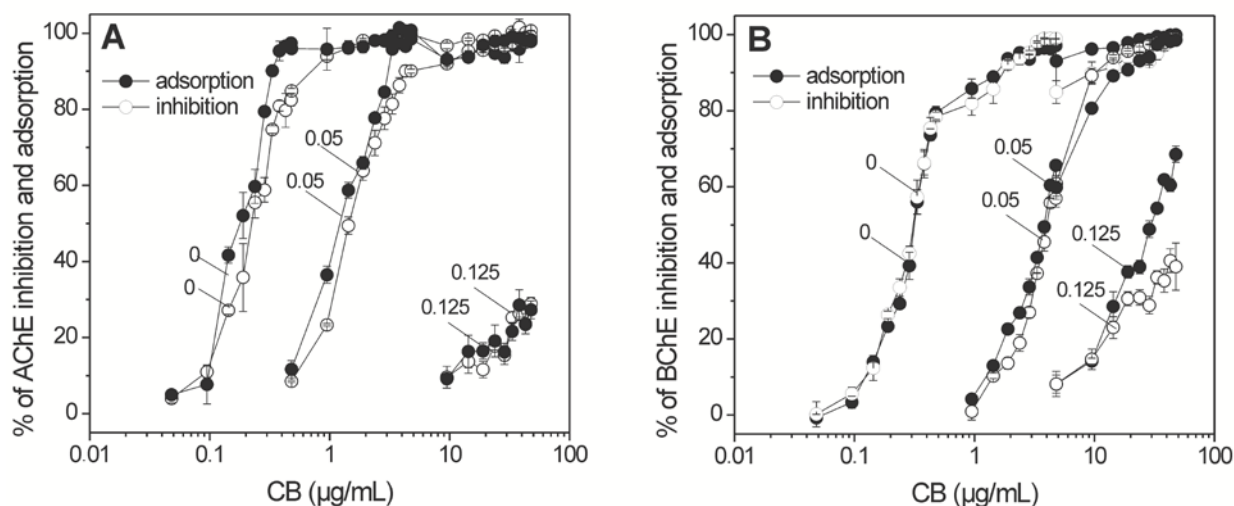


Fig. 3. Adsorption and inhibition rates of *Electrophorus electricus* AChE (A) or equine serum BChE (B) by different concentrations of uncoated and BSA-coated CB (0.048 - 47.6 µg/mL). Each point represents mean \pm SE of three independent experiments. Numbers on graphs represent the concentration of BSA (in mg/mL) used for coating the nanomaterials. For incubation with BSA, 1 mg/mL stock suspension of CB was used.

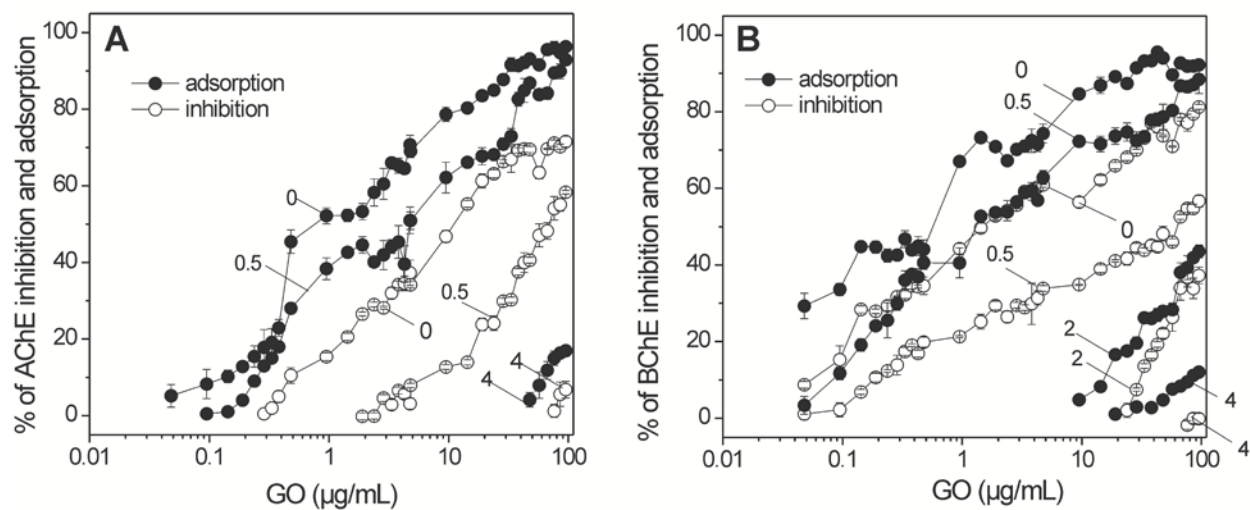


Fig. 4. Adsorption and inhibition rates of *Electrophorus electricus* AChE (A) or equine serum BChE (B) by different concentrations of uncoated and BSA-coated GO (0.048 - 95.2 µg/mL). Each point represents mean \pm SE of three independent experiments. Numbers on graphs represent the concentration of BSA (in mg/mL) used for coating the nanomaterials. For incubation with BSA, 2 mg/mL stock suspension of GO was used.

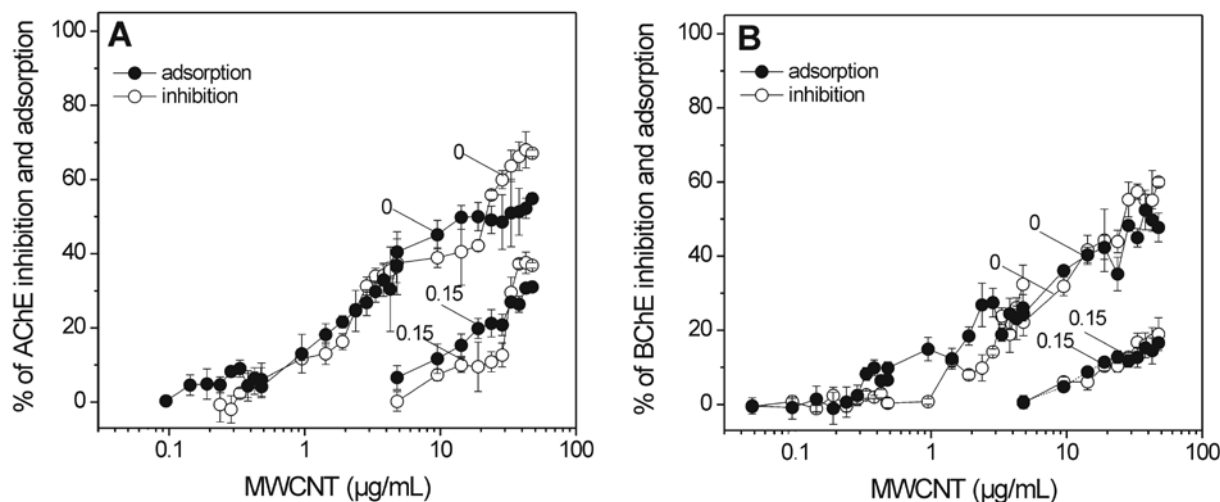


Fig. 5. Adsorption and inhibition rates of *Electrophorus electricus* AChE (**A**) or equine serum BChE (**B**) by different concentrations of uncoated and BSA-coated MWCNT (0.095 - 47.6 $\mu\text{g/mL}$). Each point represents mean \pm SE of three independent experiments. Numbers on graphs represent the concentration of BSA (in mg/mL) used for coating the nanomaterials. For incubation with BSA, 1 mg/mL stock suspension of MWCNT was used.

3.3. Effect of nanomaterials on the secondary structure of acetylcholinesterase

Circular dichroism measurements were used to determine the impact of NM on the secondary structure of AChE. A detailed inspection the far-UV CD spectra of AChE (**Fig. 6**) showed that the secondary structure of AChE was influenced by CB and GO, while MWCNT did not have any impact at the tested concentrations (**Fig. 6**, **Fig. 7**). This is consistent with the results from the enzymatic activity measurements where uncoated MWCNT also had the least effect on cholinesterases in comparison with uncoated CB or GO in a similar concentration range (**Fig. 5**). The solution of AChE was saturated with NM already at 74 $\mu\text{g/mL}$ and a further addition of NM did not have any impact on AChE secondary structure (**Fig. 7**). The CB and GO NM caused the decrease in the alpha helix content of AChE, while MWCNT did not have any effect on secondary structure elements as estimated by applying Contin deconvolution software [61] at the saturation concentration of NM (**Table 1**). It should be however noted that due to the nature of CD measurements, these tests were performed at approximately 1000 folds higher AChE:NM ratios than in the kinetic experiments, so the direct comparison of AChE:NM interactions measured by these two experimental approaches cannot be made. From our results, it can only be deduced that GO and CB induce measurable changes in the

AChE secondary structure even with enzyme: NM ratios that are considerably higher than those used in the kinetic studies. It is not excluded that MWCNT also induces secondary structure alterations of AChE, however according to the kinetic tests it is plausible that they would appear only at considerably higher MWCNT concentrations, at which recordings of CD spectra would not be possible.

Table 1. Effect of carbon-based NM (GO, CB and MWCNT; all 74 $\mu\text{g}/\text{mL}$) on the change of the secondary structure elements of *Electrophorus electricus* AChE.

NM concentration ($\mu\text{g}/\text{mL}$)	0	CB	GO	MWCNT
		74	74	74
Alpha helix (%)	9.3 \pm 1.0	7.3 \pm 1.2	6.0 \pm 1.0	8.3 \pm 0.3
Beta sheet (%)	38.3 \pm 1.0	38.3 \pm 1.2	33.7 \pm 1.3	38.7 \pm 0.9
Beta turn (%)	18.2 \pm 0.7	17.3 \pm 0.7	17.0 \pm 0.6	18.3 \pm 0.3
Remainder (%)	34.0 \pm 0.5	37.0 \pm 1.7	44.0 \pm 0.6	34.7 \pm 1.3

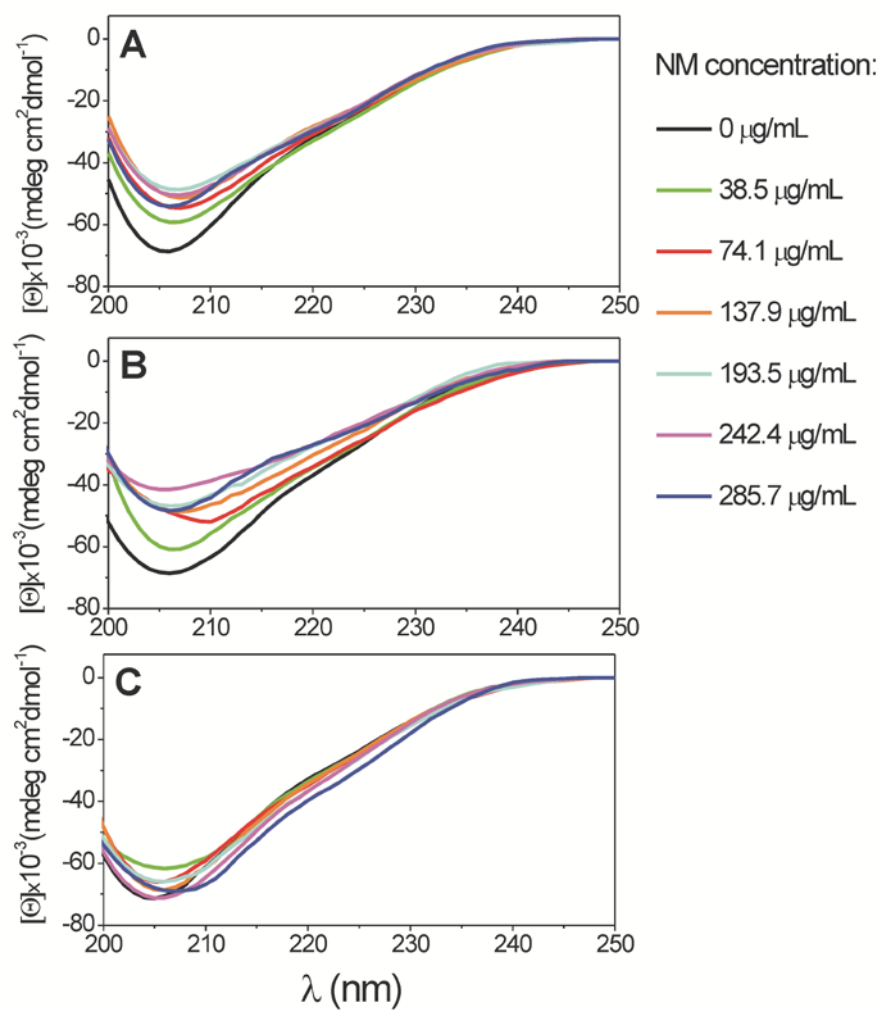


Fig. 6. Mean residue ellipticity, $[\Theta]_{205 \text{ nm}}$ of *Electrophorus electricus* AChE (0.5 mg/mL) titrated with increasing concentrations (0-285.7 μ g/mL) of CB (A), GO (B) or MWCNT (C) at 25 °C and pH 8.0.

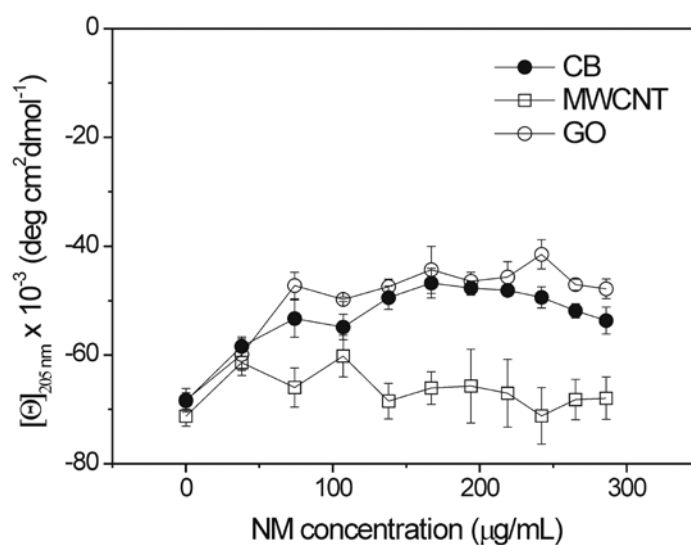


Fig. 7. Mean residue ellipticity at 205 nm, $[\Theta]_{205\text{nm}}$, of *Electrophorus electricus* AChE (0.5 mg/mL), titrated with increasing concentrations of NM (0-285.7 $\mu\text{g/mL}$) at 25 °C and pH 8.0.

3.4. Nanomaterial interaction with serum proteins

3.4.1. Impact of nanomaterials on the activity of intrinsic butyrylcholinesterase in human serum

Since in our previous experiments BSA was shown to protect the carbon-based NM from their interaction with cholinesterases, we wanted to assess whether similar effects will occur upon the addition of these NM directly to the serum which already contains soluble BChE [63]. Indeed, the titration of 0.4 % human serum with an increasing concentration of NM, and a consequent interaction of these NM with serum proteins, resulted in a large reduction of NM adsorption on BChE, and a reduced inhibition of its activity by the carbon-based NM (**Fig. 8**). The adsorption and inhibition of BChE by CB or MWCNT was almost totally abolished by the adsorption of serum proteins within the entire concentration range of the tested NM (4.8 – 476 $\mu\text{g/mL}$ mg/mL). On the contrary, and in line with the results obtained with enzyme experiments in which pure BSA was used for pre-coating (**Fig 3-5**), GO was found to be less affected by serum proteins, and had still retained its sorptive and inhibitory potential for BChE.

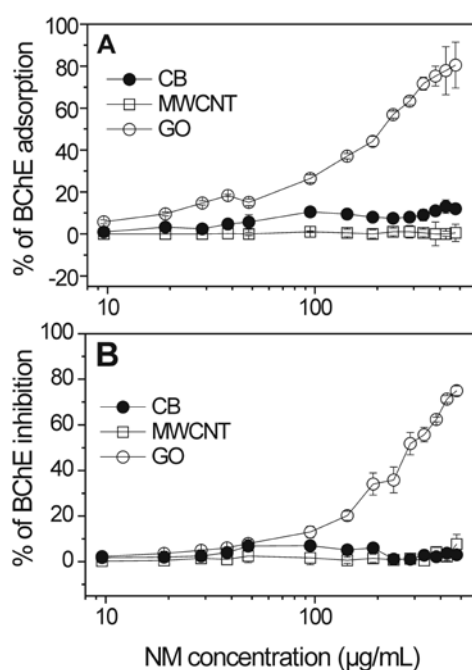


Fig. 8. – Adsorption (A) and inhibition (B) rates of BChE in 0.4 % human serum by different concentrations of NM (9.6-476 µg/mL). Each point represents mean \pm SE of three independent experiments. The final concentration of serum proteins in the reaction mixture was 0.093 mg/mL.

3.4.2. Interactions of carbon-based nanomaterials with human serum proteins

In order to establish the composition of the protein corona of the carbon-based NM, which is a consequence of NM incubation in the human serum, the NM-bound proteins were separated by 1D SDS-PAGE gel electrophoresis. Afterwards, the protein spots that appeared the most pronounced on the SDS-PAGE gel after NM incubation in the highly diluted serum (10 % and 20 %), thus representing the proteins with the highest avidity towards the NM, were analyzed by LC-ESI-MS, together with the more prominent protein spots on the SDS-PAGE gel after NM incubation in the less diluted serum (50 %), representing the most abundant serum proteins. A list of the most abundant corona serum proteins from excised protein spots is presented in **Table 2**, and the whole array of the analyzed corona proteins is presented in the supporting information (**Supporting file 1**). The SDS-PAGE separation shows that GO bound most of the proteins and that it is also the least selective (**Fig. 9**). The remarkable exception, as compared to CB and SWCNT, was the binding of serum albumin, the most abundant serum protein [64], which is visible at 55-60 kDa on the SDS-PAGE gel, and that bound to GO in

considerably lower amounts than to CB or MWCNT (**Fig. 9**). Another abundant serum protein, IgG (visible at ~250 kDa on the SDS-PAGE gel), bound to all three investigated NM (**Fig. 9, Table 2**). Several protein bands that were hardly visible after the separation of a 2 % human serum with the SDS-PAGE were enriched in the protein corona, especially complement factors and apolipoproteins (**Table 2, Fig. 9**). CB and MWCNT showed a similar binding pattern, CB being visually more sorptive (**Fig. 9**). In comparison to CB or MWCNT, more complement components and blood coagulation proteins were identified in the GO corona (**Table 2, Fig. 9**).

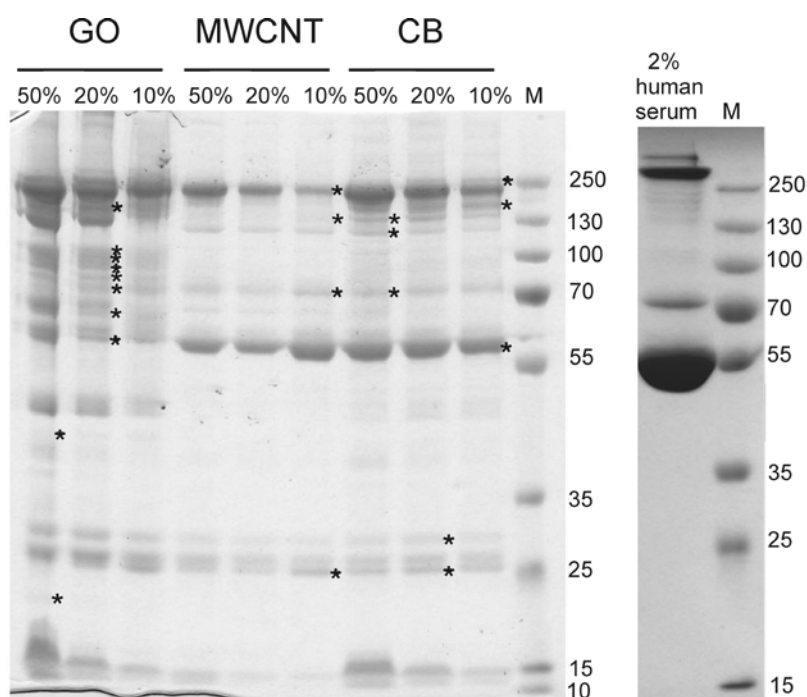


Fig. 9. SDS-PAGE analysis of human serum proteins adsorbed to carbon-based NM upon a 60-minute incubation. The human serum (50 %, 20 % and 10 % v/v in erythrocyte buffer) was incubated with 0.2 mg/mL GO or 0.5 mg/mL MWCNT or CB for 1 hour at 37 °C. The samples were then centrifuged, the supernatants removed and the pellets washed three times. Bound proteins were analyzed with the SDS-PAGE electrophoresis. Lanes: GO: 50 % (10 μ L GO and 90 μ L 50 % serum), 20 % (10 μ L GO and 90 μ L 20 % serum), 10 % (10 μ L GO and 90 μ L 10 % serum); MWCNT: 50 % (25 μ L MWCNT and 75 μ L 50 % serum), 20 % (25 μ L MWCNT and 75 μ L 20 % serum), 10 % (25 μ L MWCNT and 75 μ L 10 % serum); CB: 50 % (25 μ L CB and 75 μ L 50 % serum), 20 % (25 μ L CB and 75 μ L 20 % serum), 10 % (25 μ L CB and 75 μ L 10 % serum); 2 % human serum – 2 % serum without NM; M – molecular weight markers (kDa). Asterisks mark the analyzed protein spots.

Table 2. List of most abundant serum proteins found in the corona of carbon-based nanomaterials from the 22 excised protein spots analyzed by mass spectrometry. +++ - very abundant; ++ - abundant; + - present (according to Mascot protein score: +++ > 150 > ++ > 100 > +).

Protein name	MW (Da)	Ip	CB	CNT	GO	Functional group	Function
Serum albumin	66437	4.7	+++	+++	++	Transport	Transport protein, osmotic pressure
Serotransferrin	77064	6.81	+++	+++	+++	Transport	Transport of iron
Apolipoprotein A-I	30778	5.56	++	+++	++	Transport	Transport of cholesterol
Apolipoprotein E	36154	5.65	+	+	+++	Transport	Transport of lipoproteins
Hemopexin	51676	6.55			++	Transport	Transport of heme
Inter-alpha-trypsin inhibitor heavy chain H2	106463	5.75		++	+	Transport	Transport of hyaluronan
Inter-alpha-trypsin inhibitor heavy chain H1	101389	6.31			+	Transport	Transport of hyaluronan
Apolipoprotein A-IV	45399	5.28			+	Transport	Transport of cholesterol, antioxidant
Complement C3	184342	5.7	+++		+++	Immune system	Complement activation
Complement C4-A	192789	6.66	+++	+	++	Immune system	Complement activation
Complement component C9	63173	5.43			+++	Immune system	Complement activation, pore-forming subunit of the MAC
Inter-alpha-trypsin inhibitor heavy chain H4	103357	6.51	+	+	+++	Immune system	Acute-phase response
Complement component C8 alpha chain	65163	6.07			+++	Immune system	Complement activation, constituent of the MAC
Complement component C8 beta chain	67047	8.5			+++	Immune system	Complement activation, constituent of the MAC
Complement C1s subcomponent	76684	4.86	+	+	+++	Immune system	Complement activation

Complement component C7	93518	6.09			+++	Immune system	Complement activation, constituent of the MAC
IgG1	146000	8.6	++	+++	++	Immune system	Complement activation, antigen binding
Complement C1q subcomponent subunit B	26722	8.83	++		++	Immune system	Complement activation
Complement factor I	65750	7.72			++	Immune system	Complement activation
Complement factor B	85533	6.67			++	Immune system	Complement activation
Ig kappa	11609	5.58	++	+	+	Immune system	Complement activation, antigen binding
Complement C1r subcomponent	80119	5.89			++	Immune system	Complement activation
C1-inhibitor	55154	6.09			++	Immune system	Complement regulation, fibrinolysis regulation
Ig alpha	37655	6.08	++	+	+	Immune system	Antigen binding
Complement component C6	104786	6.39			+	Immune system	Complement activation, constituent of MAC
Alpha-1-antichymotrypsin	47651	5.33			+	Immune system	Acute-phase response
Ig gamma-2 chain C region	35901	7.66	+			Immune system	Complement activation, antigen binding
Lipopolysaccharide-binding protein	53384	6.4			+	Immune system	Acute-phase response
Complement component C8 gamma chain	22277	8.49			+	Immune system	Complement activation, constituent of MAC
Alpha-1-antitrypsin	46737	5.37			+	Immune system	Acute-phase response, blood coagulation
Ig gamma-3 chain C region	41287	8.23		+		Immune system	Complement activation, antigen binding
Complement factor H-related protein 1	37650	7.39	+		+	Immune system	Complement activation
Ig lambda-1 chain C regions	11384	7.89	+	+	+	Immune system	Complement activation, antigen binding
Complement factor H	139096	6.21			+	Immune system	Complement regulation
Complement C1q subcomponent subunit C	25774	8.61			+	Immune system	Complement activation
Vitamin K-dependent protein S	75123	5.0-5.5		+++	+	Haemostasis	Anticoagulant

Coagulation factor IX	51778	4.2-4.5			++	Haemostasis	Blood coagulation
Carboxypeptidase B2	48424	7.61			++	Haemostasis	Blood coagulation
Tetranectin	22537	5.52			++	Haemostasis	Fibrinolysis
Prothrombin	70037	5.64			++	Haemostasis	Blood coagulation
Antithrombin-III	52602	4.9-5.3	+		++	Haemostasis	Blood coagulation inhibition
Kininogen-1	71957	6.34	+		+	Haemostasis	Blood coagulation inhibition
Kallistatin	48542	5			+	Haemostasis	Blood pressure regulation, vascular remodelling
Plasminogen	90569	7.04			+	Haemostasis	Fibrinolysis
Coagulation factor XII	67792	8.04			+	Haemostasis	Blood coagulation
Vitronectin	54306	5.55	+		++	Tissue structuring	Extracellular matrix binding
Fibulin-1	77214	5.11			++	Tissue structuring	Extracellular matrix organization
Gelsolin	85698	5.83			++	Tissue structuring	Fibronectin binding
Hyaluronan-binding protein 2	62672	6.09			+	Tissue structuring	Cell adhesion, hyaluronan binding
Clusterin	52495	5.89	++	++	+	Cell death	Chaperone, prevents protein aggregation
Glutathione peroxidase 3	25552	8.26			+	Oxidative stress	Oxidative stress

4. Discussion

The carbon-based NM are among the most sorptive NM [23,35,36] and have the capability to bind many different proteins to their surface [17,18,46,65,66]. This fact is beneficial when NM are used as scaffolds, but can also be disadvantageous when NM are introduced into the body and come in contact with different biological media. Here, most sorptive NM may adsorb and affect more proteins.

4.1. *Interaction of NM with BSA and cholinesterases*

The study presented here shows that, when GO, CB or MWCNT in their pristine (uncoated) forms were incubated with cholinesterases, the adsorption and the inhibition of the enzyme was the lowest with MWCNT. We explain this as a result of a higher surface curvature of MWCNT as compared to GO and CB. Mesarič et al. [56] observed a similar trend with fullerenes C₆₀, which have an even higher surface curvature, and which formed a considerably lower number of atomic contacts with insect AChE in comparison to CB or GO. Enhanced protein adsorption capacity on flatter surfaces, and consequent structural changes of the adsorbed proteins, was also reported also by other authors. For example, computer simulation studies of Balamurugan et al. [50] revealed that a lower surface curvature of carbon-based NM increases the protein α -helical breaking tendency. Similarly, Mu et al. [13] showed experimentally that lowering the surface curvature of MWCNTs can induce larger protein conformational changes. Increased protein adsorption capacity on carbon-based NM with flatter surfaces was confirmed also by Zuo et al. [16] and Gu et al. [67]. All these studies on carbon-based NM are consistent also with previous findings on spherical silica NM [47,48] as well as with our CD-spectroscopy results, which showed that CB and GO with a lower surface curvature decreased the α -helical content (and in the case of GO also decreased the content of β -sheets), while MWCNT with a higher surface curvature did not induce this or any other changes in the secondary structure of electric eel AChE.

The pre-coating of NM in protein solutions may substantially modify the NM interactions with biological molecules. In the study by Mesarič et al. [56], as well as in our experiments with uncoated NM, GO showed a high sorptive potential for cholinesterases, but a low inhibitory potential. However, when carbon-based NM were pre-coated with BSA, significantly higher (13- to 16-fold) concentrations of BSA were needed for GO in comparison with MWCNT or CB, respectively, to diminish the impact of the NM on the inhibition of AChE and BChE. This indicates that the binding affinity of BSA towards GO is

much lower than towards CB or MWCNT, allowing cholinesterases to adsorb to GO. To what extent the pre-incubation of specific proteins may modify the fate of NM in the body remains a matter of further research.

4.2. Protein corona of carbon-based NM after incubation with human serum proteins

The composition of the NM protein corona modulates the NM biocompatibility and distribution within the body. Complement factors, immunoglobulins and fibronectin are involved in the NM opsonisation and their translocation to liver and spleen [31,68], while the binding of serum albumin prolongs the NM circulation time in blood [69,70], and the attachment of apolipoproteins facilitates the translocation of NM through the blood brain barrier [29, 30]. In addition, proteins involved in hyaluronan binding promote the NM-cell association [71].

In our study, GO was found to bind considerably higher amounts of serum proteins in comparison with CB or MWCNT, as shown by the stronger intensity of protein bands at lower GO concentrations (**Fig. 9**). This could be a consequence of the low surface curvature of GO, combined with the presence of its negatively charged functional groups, resulting in both hydrogen binding and electrostatic interactions [56], in addition to hydrophobic and van der Waals interactions, which govern the adsorption of serum proteins on CB [56] and CNT [16,50]. In line with these findings, the NM with the highest surface curvature, MWCNT, was found to bind the least amount of proteins.

We suggest that these observed differences in the corona composition are not only due to different aggregation status of tested the NM. Namely, the adsorption of proteins onto carbon-based NM is dictated by hydrophobic and π - π interactions between aliphatic and aromatic residues and the conjugated NM surface. Accordingly, protein adsorption is highly sensitive to topological constraints imposed by carbon-based NM surface structure; in particular, adsorption capacity is thought to increase as the incident surface curvature decreases [56][67]. Further, if we hypothesize that the differences in the adsorption and inhibition of cholinesterases to the tested NM are solely due to the differences in surface area available, one would expect that the ratio between the inhibition and adsorption potential would be similar in all the tested NM. Also, the shape of the adsorption/inhibition curves would be the same in all the cases. In our study, this is not the case. Enzymes adsorbed to GO are still active, while this is not the case when they are adsorbed to CB and MWCNT. However, in cases of the BSA pre-treatment, the surface of NM is covered by BSA, resulting in fewer

surfaces available for enzyme adsorption in the same type of NM. Here the different amount of adsorbed surfaces indeed resulted in same shape of curves (Figs. 3-5). These combined results indicate that the interactions of cholinesterases, as well as of the serum proteins with different NM are not solely the result of differences in NM aggregation, but are also due to different affinities of the three NM towards these proteins. Finally, serum proteins exhibited different binding patterns to three investigated NM (**Fig. 9**), thus we take this as an indication of different affinities of investigated NM for the serum proteins, and not only as the consequence of different amounts of binding surfaces. There are even some proteins (see for example the ~50 kDa protein band on **Fig. 9**) which are bound only to one type of NM, but not to the other two.

The competition of proteins for the adsorption on the surface of NM, which is affected by incubation time, protein concentration, and adsorption affinity between a protein and the NM surface, is called the “Vroman effect” [72]. More abundant proteins, such as serum albumin, may dominate on the NM surface after short incubation periods, but will subsequently be replaced by lower abundance proteins with a higher affinity and a slower binding kinetics [5]. The amount of proteins in the protein corona of carbon-based NM becomes stable after only 5 minutes of incubation for MWCNT and CB [8], and after 30 minutes of incubation for GO [9]. When SWCNT were incubated with a mixture of BSA and bovine fibrinogen, no notable change in the adsorption ratio of the two proteins was visible after a 60 minute incubation, compared to longer incubation periods [37]. Similarly, when CB was incubated with a mixture of BSA, bovine fibrinogen and bovine IgG, the ratio between the three adsorbed proteins was stable after 15 minutes and up to 24 hours [23]. Therefore, we assume that the 60 minute incubation time of NM with the human serum in our study was long enough for the formation of a stable protein corona.

The most abundant serum protein, serum albumin [64], was bound to all three investigated NM, but to GO in lesser amounts as shown by the SDS-PAGE (**Fig. 9**) and mass spectrometry analyses (**Table 2**). Because of its oxygen-containing functional groups, GO is less hydrophobic than CB or MWCNT, and hydrophobic NM were shown to adsorb more albumin molecules than hydrophilic ones [73]. This specific, significantly weaker affinity of BSA towards GO compared to CB or MWCNT was further confirmed by the experiment in which we took advantage of the intrinsic serum BChE, which will compete with serum albumin and other less abundant serum proteins for binding on the NM surface. We measured the inhibition of BChE activity as an indicator of BChE interaction with the NM. The adsorption

of serum proteins on CB or MWCNT resulted in a complete retention of BChE activity, indicating that other serum proteins, but not BChE, had a high affinity towards CB and MWCNT. On the other hand, GO inhibited the activity of the intrinsic serum BChE, confirming BChE adsorption. We explain this with different preferential binding of serum albumin to CB, MWCNT and GO. Serum albumin, being the most abundant serum protein [64], is most probably responsible for the formation of the corona which prevents BChE adsorption on CB and MWCNT. However, the weaker affinity of albumin towards GO seems to be responsible for the adsorption of the less abundant serum proteins on the GO surface (**Fig. 9**). Among them is also BChE, as shown by the inhibition of its enzymatic activity in the serum (**Fig. 8**). Our results indicate that some NM, when coated with a protein corona, can affect both the structure and function of the less abundant but physiologically important adsorbed serum proteins. Whether BChE binds directly to the NM surface or forms a secondary corona on the primary one, remains unresolved.

The proteins identified in the excised SDS-PAGE gel spots are mainly involved in transport and immune response (**Table 2**). The abundant serum proteins exhibiting these functions, for example immunoglobulin IgG1 and serotransferrin (the precursor of transferrin), were found bound to all investigated NM. The proteins that were enriched in the protein corona of all investigated NM as compared to their amounts in the serum, were mainly complement factors and apolipoproteins. A particularly high number of many different complement factors was identified in the excised gel spots of the GO corona, together with proteins involved in haemostasis and tissue structuring. The role of the more prominent protein groups and the possible consequences arising from their interaction with NM are discussed in detail below.

More complement components were identified in the corona of GO than of CB or MWCNT, though some complement components (for example complement C4-A) were identified on all of the three investigated NM. Both GO and CB bound the complement C3 precursor and complement C1q precursor. The complement system plays a central role in the modulation of immune and inflammatory responses towards intruders and may be the key contributing factor in eliciting acute allergic responses to NM and nanomedicines. It can be activated by three different pathways that converge at the cleavage of the central complement protein C3 [74]. The classical pathway of the complement is initiated by the binding of the C1q recognition molecule to the surface of NM [39], while direct interaction with C3 and C4 molecules could cause a conformational change of these proteins, leading to the products resembling activated C3 and C4 [74]. Hydroxyl groups, such as those on the surface of GO, are capable of a

nucleophilic attack on the internal thioester bond in the α -chain of nascent C3b, thereby accelerating a complement alternative pathway turnover [74]. Feng et al. [46] discovered that the concentration of complement protein fragments C3a and C5a was increased in human plasma in the presence of GO compared to the control (phosphate saline buffer), further proving the ability of GO to activate the complement system. CNT were reported to activate the complement system *via* the classical pathway, or *via* the lecithin activation pathway [39]. SWCNT and double-walled CNT activate the complement system *via* a classical pathway, and double-walled CNT trigger the alternative activation pathway as well [38].

Apolipoproteins, such as apolipoprotein E, apolipoprotein A-I and apolipoprotein B-100, can facilitate the translocation of different NM through the blood brain barrier [33,34]. The attachment of apolipoproteins can also be used for targeting cells with lipoprotein receptors [28]. Apolipoproteins A-I tends to bind to more hydrophobic NM [5]. The binding of apolipoprotein A to the carbon-based NM, namely SWCNT, double-walled CNT, MWCNT and CB has been reported previously [18,23,38,65]. In our study, all the investigated carbon-based NM adsorbed apolipoprotein A-I and apolipoprotein E to their surface, indicating these NM as suitable candidates for drug transport through the blood brain barrier, or on the other hand presenting a serious threat of uncontrolled penetration of these NM into the brain.

Immunoglobulins are globular glycoprotein molecules that play an essential role in the immune system. They are divided into classes that have different concentrations in serum (IgG > IgA > IgM > IgD > IgE) [17]. IgG has the role in antigen binding and complement activation, where it activates the classical pathway [74], and acts as an opsonin, promoting the removal of NM from the systemic circulation and their phagocytosis. It preferentially binds on negatively charged NM bearing strong basic or weak acid groups on their surface [75]. In our study, IgG1 bound to all three investigated NM. Other studies also confirm the presence of IgG in the carbon-based NM corona, namely CB and PEG-SWCNT [17, 23].

We have also found that serotransferrin, the transferrin precursor, binds to all three investigated NM in relatively high amounts (**Table 2**). Transferrin is a non-heme iron-binding glycoprotein. The transferrin receptor-mediated endocytosis is a major route of cellular iron uptake and this has been exploited for the site-specific drug and gene delivery [76], so the carbon-based NM could be considered as potential candidates for the transferrin receptor-mediated endocytosis.

Hyaluronan-binding proteins, namely inter-alpha-trypsin inhibitor heavy chain H1, H2 and hyaluronan-binding protein 2, were identified in the corona of GO and MWCNT. These

proteins promote NM cell association – adhesion to the cell membrane and the internalization of the NM [71].

In order to test the suitability of different NM as drug carriers, the characterisation of the dispersions of these NM is of high importance. At present, there is however no consensus on the methods used for characterisation of nanoparticles in biological suspensions (NanoValid; <http://www.nanovalid.eu/>) for the purposes of bio-nano studies. The choice of methods for NM characterisation is limited to scanning electron microscopy, transmission electron microscopy, energy-dispersive X-ray spectroscopy, DLS and zeta potential measurements. Among them, only DLS measures the state of dispersion; but even this measurement has limitations since it is designed for stable suspensions. In addition, the agglomeration of NM is a time-dependent “on-off” dynamic process, while DLS measurement describes the situation only in a certain time point. Due to these facts, quite some authors have presented indirect approaches for description of characteristics of NM in a suspension. Xia et al [35] have elaborated the biological surface adsorption indices and nanodescriptors for characterization of NM in biological systems, while Meng and Ugaz [77] have suggested a physico-chemical analyses of suspensions of NM based on the fluorescence signature of NM that is independent of their agglomeration state. We suggest that adsorption/inhibition of proteins on the surface of NN may also provide data on adsorption potential of the NM suspension in time.

In the view of possible use of the carbon-based NM as drug delivery systems, our results indicate that GO would be a less suitable candidate in comparison with the other two hydrophobic NM in terms of the circulation time in blood. Its considerably lower interaction with serum albumin, which is known to prolong the NM circulation time in blood, as well as its strong interaction with molecules involved in the protein clearance (especially complement factors), make GO potentially more prone to opsonisation and clearance from the blood circulation than CB or MWCNT. In addition, GO binds a broader spectrum of serum proteins which could increase the side effects of this NM by altering the physiological function of these proteins. At present, these are however only hypotheses deduced from our results that have to be further confirmed *in vivo*.

Conclusions

The results of this study show that the binding affinity of three tested carbon-based NM towards serum albumin in a pure albumin solution is preserved in the mixture of serum proteins. CB and MWCNT have comparable affinities towards serum albumin, which are

considerably higher than the affinity of GO. Next, GO shows a much higher sorptive capacity and a lower binding specificity for other serum proteins, and consequently binds a broader spectrum of serum proteins. The protein corona of the investigated carbon-based NM after the incubation in the human serum is enriched with complement factors and apolipoproteins. GO corona also contains less abundant serum proteins, including intrinsic serum BChE whose activity is altered due to the adsorption. These results indicate that NM with a high sorptive capacity and a low affinity towards serum albumin could affect the function of less abundant serum proteins.

Acknowledgements

This investigation was supported under the grant “Innovative scheme of co-funding doctoral studies for promoting co-operation with the economy and solving of contemporary social challenges”, operation part financed by the European Union, European Social Fund and the Republic of Slovenia, Ministry for Education, Science and Sport in the framework of the Operational programme for human resources development for the period 2007 – 2013. It was also supported by European Community's Seventh Framework Project NanoMile (NMP4-LA-2013-310451), and by the Slovenian Research Agency (grant P1-0207).

References

- [1] Duncan R, Gaspar R. Nanomedicine(s) under the Microscope. *Mol Pharm* 2011;8:2101–41. doi:10.1021/mp200394t.
- [2] Mahon E, Salvati A, Baldelli Bombelli F, Lynch I, Dawson KA. Designing the nanoparticle–biomolecule interface for “targeting and therapeutic delivery.” *J Controlled Release* 2012;161:164–74. doi:10.1016/j.jconrel.2012.04.009.
- [3] Liu J, Cui L, Losic D. Graphene and graphene oxide as new nanocarriers for drug delivery applications. *Acta Biomater* 2013;9:9243–57. doi:10.1016/j.actbio.2013.08.016.
- [4] Goenka S, Sant V, Sant S. Graphene-based nanomaterials for drug delivery and tissue engineering. *J Controlled Release* 2014;173:75–88. doi:10.1016/j.jconrel.2013.10.017.
- [5] Cedervall T, Lynch I, Lindman S, Berggård T, Thulin E, Nilsson H, et al. Understanding the nanoparticle–protein corona using methods to quantify exchange rates and affinities of proteins for nanoparticles. *Proc Natl Acad Sci* 2007;104:2050–5. doi:10.1073/pnas.0608582104.
- [6] Monopoli MP, Åberg C, Salvati A, Dawson KA. Biomolecular coronas provide the biological identity of nanosized materials. *Nat Nanotechnol* 2012;7:779–86.

doi:10.1038/nnano.2012.207.

- [7] Lundqvist M, Stigler J, Cedervall T, Berggård T, Flanagan MB, Lynch I, et al. The Evolution of the Protein Corona around Nanoparticles: A Test Study. *ACS Nano* 2011;5:7503–9. doi:10.1021/nn202458g.
- [8] Zhu Y, Li W, Li Q, Li Y, Li Y, Zhang X, et al. Effects of serum proteins on intracellular uptake and cytotoxicity of carbon nanoparticles. *Carbon* 2009;47:1351–8. doi:10.1016/j.carbon.2009.01.026.
- [9] Hu W, Peng C, Lv M, Li X, Zhang Y, Chen N, et al. Protein Corona-Mediated Mitigation of Cytotoxicity of Graphene Oxide. *ACS Nano* 2011;5:3693–700. doi:10.1021/nn200021j.
- [10] Lesniak A, Fenaroli F, Monopoli MP, Åberg C, Dawson KA, Salvati A. Effects of the Presence or Absence of a Protein Corona on Silica Nanoparticle Uptake and Impact on Cells. *ACS Nano* 2012;6:5845–57. doi:10.1021/nn300223w.
- [11] Lesniak A, Salvati A, Santos-Martinez MJ, Radomski MW, Dawson KA, Åberg C. Nanoparticle Adhesion to the Cell Membrane and Its Effect on Nanoparticle Uptake Efficiency. *J Am Chem Soc* 2013;135:1438–44. doi:10.1021/ja309812z.
- [12] Lynch I, Dawson KA. Protein-nanoparticle interactions. *Nano Today* 2008;3:40–7. doi:10.1016/S1748-0132(08)70014-8.
- [13] Mu Q, Liu W, Xing Y, Zhou H, Li Z, Zhang Y, et al. Protein Binding by Functionalized Multiwalled Carbon Nanotubes Is Governed by the Surface Chemistry of Both Parties and the Nanotube Diameter. *J Phys Chem C* 2008;112:3300–7. doi:10.1021/jp710541j.
- [14] Dell’Orco D, Lundqvist M, Oslakovic C, Cedervall T, Linse S. Modeling the Time Evolution of the Nanoparticle-Protein Corona in a Body Fluid. *PLoS ONE* 2010;5:e10949. doi:10.1371/journal.pone.0010949.
- [15] Tenzer S, Docter D, Rosfa S, Wlodarski A, Kuharev J, Rekić A, et al. Nanoparticle Size Is a Critical Physicochemical Determinant of the Human Blood Plasma Corona: A Comprehensive Quantitative Proteomic Analysis. *ACS Nano* 2011;5:7155–67. doi:10.1021/nn201950e.
- [16] Zuo G, Zhou X, Huang Q, Fang H, Zhou R. Adsorption of Villin Headpiece onto Graphene, Carbon Nanotube, and C60: Effect of Contacting Surface Curvatures on Binding Affinity. *J Phys Chem C* 2011;115:23323–8. doi:10.1021/jp208967t.
- [17] Sacchetti C, Motamedchaboki K, Magrini A, Palmieri G, Mattei M, Bernardini S, et al. Surface Polyethylene Glycol Conformation Influences the Protein Corona of Polyethylene Glycol-Modified Single-Walled Carbon Nanotubes: Potential Implications on Biological Performance. *ACS Nano* 2013;7:1974–89. doi:10.1021/nn400409h.

- [18] Shannahan JH, Brown JM, Chen R, Ke PC, Lai X, Mitra S, et al. Comparison of Nanotube–Protein Corona Composition in Cell Culture Media. *Small* 2013;9:2171–81. doi:10.1002/sml.201202243.
- [19] Deng ZJ, Mortimer G, Schiller T, Musumeci A, Martin D, Minchin RF. Differential plasma protein binding to metal oxide nanoparticles. *Nanotechnology* 2009;20:455101. doi:10.1088/0957-4484/20/45/455101.
- [20] Dobrovolskaia MA, Patri AK, Zheng J, Clogston JD, Ayub N, Aggarwal P, et al. Interaction of colloidal gold nanoparticles with human blood: effects on particle size and analysis of plasma protein binding profiles. *Nanomedicine Nanotechnol Biol Med* 2009;5:106–17. doi:10.1016/j.nano.2008.08.001.
- [21] Monopoli MP, Walczyk D, Campbell A, Elia G, Lynch I, Baldelli Bombelli F, et al. Physical–Chemical Aspects of Protein Corona: Relevance to in Vitro and in Vivo Biological Impacts of Nanoparticles. *J Am Chem Soc* 2011;133:2525–34. doi:10.1021/ja107583h.
- [22] Mahmoudi M, Lynch I, Ejtehadi MR, Monopoli MP, Bombelli FB, Laurent S. Protein-nanoparticle interactions: opportunities and challenges. *Chem Rev* 2011;111:5610–37.
- [23] Ruh H, Kühl B, Brenner-Weiss G, Hopf C, Diabaté S, Weiss C. Identification of serum proteins bound to industrial nanomaterials. *Toxicol Lett* 2012;208:41–50. doi:10.1016/j.toxlet.2011.09.009.
- [24] Åkesson A, Cárdenas M, Elia G, Monopoli MP, Dawson KA. The protein corona of dendrimers: PAMAM binds and activates complement proteins in human plasma in a generation dependent manner. *RSC Adv* 2012;2:11245. doi:10.1039/c2ra21866f.
- [25] Cai X, Ramalingam R, Wong HS, Cheng J, Ajuh P, Cheng SH, et al. Characterization of carbon nanotube protein corona by using quantitative proteomics. *Nanomedicine Nanotechnol Biol Med* 2013;9:583–93. doi:10.1016/j.nano.2012.09.004.
- [26] Schäffler M, Semmler-Behnke M, Sarioglu H, Takenaka S, Wenk A, Schleh C, et al. Serum protein identification and quantification of the corona of 5, 15 and 80 nm gold nanoparticles. *Nanotechnology* 2013;24:265103. doi:10.1088/0957-4484/24/26/265103.
- [27] Walkey CD, Olsen JB, Guo H, Emili A, Chan WCW. Nanoparticle Size and Surface Chemistry Determine Serum Protein Adsorption and Macrophage Uptake. *J Am Chem Soc* 2012;134:2139–47. doi:10.1021/ja2084338.
- [28] Barrán-Berdón AL, Pozzi D, Caracciolo G, Capriotti AL, Caruso G, Cavaliere C, et al. Time Evolution of Nanoparticle–Protein Corona in Human Plasma: Relevance for Targeted Drug Delivery. *Langmuir* 2013;29:6485–94. doi:10.1021/la401192x.
- [29] Jedlovsky-Hajdú A, Bombelli FB, Monopoli MP, Tombácz E, Dawson KA. Surface Coatings Shape the Protein Corona of SPIONs with Relevance to Their Application in Vivo. *Langmuir* 2012;28:14983–91. doi:10.1021/la302446h.

- [30] Lartigue L, Wilhelm C, Servais J, Factor C, Dencausse A, Bacri J-C, et al. Nanomagnetic Sensing of Blood Plasma Protein Interactions with Iron Oxide Nanoparticles: Impact on Macrophage Uptake. *ACS Nano* 2012;6:2665–78. doi:10.1021/nn300060u.
- [31] Aggarwal P, Hall JB, McLeland CB, Dobrovolskaia MA, McNeil SE. Nanoparticle interaction with plasma proteins as it relates to particle biodistribution, biocompatibility and therapeutic efficacy. *Adv Drug Deliv Rev* 2009;61:428–37. doi:10.1016/j.addr.2009.03.009.
- [32] Nagayama S, Ogawara K, Fukuoka Y, Higaki K, Kimura T. Time-dependent changes in opsonin amount associated on nanoparticles alter their hepatic uptake characteristics. *Int J Pharm* 2007;342:215–21. doi:10.1016/j.ijpharm.2007.04.036.
- [33] Kim HR, Andrieux K, Delomenie C, Chacun H, Appel M, Desmaële D, et al. Analysis of plasma protein adsorption onto PEGylated nanoparticles by complementary methods: 2-DE, CE and Protein Lab-on-chip® system. *ELECTROPHORESIS* 2007;28:2252–61. doi:10.1002/elps.200600694.
- [34] Kreuter J, Hekmatara T, Dreis S, Vogel T, Gelperina S, Langer K. Covalent attachment of apolipoprotein A-I and apolipoprotein B-100 to albumin nanoparticles enables drug transport into the brain. *J Controlled Release* 2007;118:54–8. doi:10.1016/j.jconrel.2006.12.012.
- [35] Xia XR, Monteiro-Riviere NA, Mathur S, Song X, Xiao L, Oldenberg SJ, et al. Mapping the Surface Adsorption Forces of Nanomaterials in Biological Systems. *ACS Nano* 2011;5:9074–81. doi:10.1021/nn203303c.
- [36] Valenti LE, Fiorito PA, García CD, Giacomelli CE. The adsorption–desorption process of bovine serum albumin on carbon nanotubes. *J Colloid Interface Sci* 2007;307:349–56. doi:10.1016/j.jcis.2006.11.046.
- [37] Ge C, Du J, Zhao L, Wang L, Liu Y, Li D, et al. Binding of blood proteins to carbon nanotubes reduces cytotoxicity. *Proc Natl Acad Sci* 2011;108:16968–73. doi:10.1073/pnas.1105270108.
- [38] Salvador-Morales C, Flahaut E, Sim E, Sloan J, H. Green ML, Sim RB. Complement activation and protein adsorption by carbon nanotubes. *Mol Immunol* 2006;43:193–201. doi:10.1016/j.molimm.2005.02.006.
- [39] Andersen AJ, Robinson JT, Dai H, Hunter AC, Andresen TL, Moghimi SM. Single-Walled Carbon Nanotube Surface Control of Complement Recognition and Activation. *ACS Nano* 2013;7:1108–19. doi:10.1021/nn3055175.
- [40] Holt BD, Dahl KN, Islam MF. Quantification of Uptake and Localization of Bovine Serum Albumin-Stabilized Single-Wall Carbon Nanotubes in Different Human Cell Types. *Small* 2011;7:2348–55. doi:10.1002/smll.201100437.

- [41] Mu Q, Su G, Li L, Gilbertson BO, Yu LH, Zhang Q, et al. Size-Dependent Cell Uptake of Protein-Coated Graphene Oxide Nanosheets. *ACS Appl Mater Interfaces* 2012;4:2259–66. doi:10.1021/am300253c.
- [42] Wu Z, Zhang B, Yan B. Regulation of Enzyme Activity through Interactions with Nanoparticles. *Int J Mol Sci* 2009;10:4198–209. doi:10.3390/ijms10104198.
- [43] Billsten P, Wahlgren M, Arnebrant T, McGuire J, Elwing H. Structural Changes of T4 Lysozyme upon Adsorption to Silica Nanoparticles Measured by Circular Dichroism. *J Colloid Interface Sci* 1995;175:77–82. doi:10.1006/jcis.1995.1431.
- [44] Karajanagi SS, Vertegel AA, Kane RS, Dordick JS. Structure and Function of Enzymes Adsorbed onto Single-Walled Carbon Nanotubes. *Langmuir* 2004;20:11594–9. doi:10.1021/la047994h.
- [45] Mandal S, Hossain M, Devi PS, Kumar GS, Chaudhuri K. Interaction of carbon nanoparticles to serum albumin: elucidation of the extent of perturbation of serum albumin conformations and thermodynamical parameters. *J Hazard Mater* 2013;248–249:238–45. doi:10.1016/j.jhazmat.2013.01.009.
- [46] Feng R, Yu Y, Shen C, Jiao Y, Zhou C. Impact of graphene oxide on the structure and function of important multiple blood components by a dose-dependent pattern: Impact of GO on Structure and Function of Multiple Blood Components. *J Biomed Mater Res A* 2014;n/a – n/a. doi:10.1002/jbm.a.35341.
- [47] Vertegel AA, Siegel RW, Dordick JS. Silica Nanoparticle Size Influences the Structure and Enzymatic Activity of Adsorbed Lysozyme. *Langmuir* 2004;20:6800–7. doi:10.1021/la0497200.
- [48] Lundqvist M, Sethson I, Jonsson B-H. Protein Adsorption onto Silica Nanoparticles: Conformational Changes Depend on the Particles' Curvature and the Protein Stability. *Langmuir* 2004;20:10639–47. doi:10.1021/la0484725.
- [49] Yi C, Fong C-C, Zhang Q, Lee S-T, Yang M. The structure and function of ribonuclease A upon interacting with carbon nanotubes. *Nanotechnology* 2008;19:095102. doi:10.1088/0957-4484/19/9/095102.
- [50] Balamurugan K, Singam ERA, Subramanian V. Effect of Curvature on the α -Helix Breaking Tendency of Carbon Based Nanomaterials. *J Phys Chem C* 2011;115:8886–92. doi:10.1021/jp110898r.
- [51] Podila R, Vedantam P, Ke PC, Brown JM, Rao AM. Evidence for Charge-Transfer-Induced Conformational Changes in Carbon Nanostructure–Protein Corona. *J Phys Chem C* 2012;116:22098–103. doi:10.1021/jp3085028.
- [52] You C-C, De M, Han G, Rotello VM. Tunable Inhibition and Denaturation of α -Chymotrypsin with Amino Acid-Functionalized Gold Nanoparticles. *J Am Chem Soc* 2005;127:12873–81. doi:10.1021/ja0512881.

- [53] Xu Z, Liu X-W, Ma Y-S, Gao H-W. Interaction of nano-TiO₂ with lysozyme: insights into the enzyme toxicity of nanosized particles. *Environ Sci Pollut Res* 2010;17:798–806. doi:10.1007/s11356-009-0153-1.
- [54] Wang Z, Zhang K, Zhao J, Liu X, Xing B. Adsorption and inhibition of butyrylcholinesterase by different engineered nanoparticles. *Chemosphere* 2010;79:86–92. doi:10.1016/j.chemosphere.2009.12.051.
- [55] Wang Z, Zhao J, Li F, Gao D, Xing B. Adsorption and inhibition of acetylcholinesterase by different nanoparticles. *Chemosphere* 2009;77:67–73. doi:10.1016/j.chemosphere.2009.05.015.
- [56] Mesarič T, Baweja L, Drašler B, Drobne D, Makovec D, Dušak P, et al. Effects of surface curvature and surface characteristics of carbon-based nanomaterials on the adsorption and activity of acetylcholinesterase. *Carbon* 2013;62:222–32. doi:10.1016/j.carbon.2013.05.060.
- [57] Pohanka M. Cholinesterases, a target of pharmacology and toxicology. *Biomed Pap* 2011;155:219–23. doi:10.5507/bp.2011.036.
- [58] Wessler I, Kirkpatrick CJ. Acetylcholine beyond neurons: the non-neuronal cholinergic system in humans. *Br J Pharmacol* 2008;154:1558–71. doi:10.1038/bjp.2008.185.
- [59] Pezzementi L, Chatonnet A. Evolution of cholinesterases in the animal kingdom. *Chem Biol Interact* 2010;187:27–33. doi:10.1016/j.cbi.2010.03.043.
- [60] Li B, Stribley JA, Ticu A, Xie W, Schopfer LM, Hammond P, et al. Abundant Tissue Butyrylcholinesterase and Its Possible Function in the Acetylcholinesterase Knockout Mouse. *J Neurochem* 2000;75:1320–31. doi:10.1046/j.1471-4159.2000.751320.x.
- [61] Provencher SW, Gloeckner J. Estimation of globular protein secondary structure from circular dichroism. *Biochemistry (Mosc)* 1981;20:33–7. doi:10.1021/bi00504a006.
- [62] Leonardi A, Biass D, Kordiš D, Stöcklin R, Favreau P, Križaj I. Conus consors Snail Venom Proteomics Proposes Functions, Pathways, and Novel Families Involved in Its Venomic System. *J Proteome Res* 2012;11:5046–58. doi:10.1021/pr3006155.
- [63] Li B, Sedlacek M, Manoharan I, Boopathy R, Duysen EG, Masson P, et al. Butyrylcholinesterase, paraoxonase, and albumin esterase, but not carboxylesterase, are present in human plasma. *Biochem Pharmacol* 2005;70:1673–84. doi:10.1016/j.bcp.2005.09.002.
- [64] Chromy BA, Gonzales AD, Perkins J, Choi MW, Corzett MH, Chang BC, et al. Proteomic Analysis of Human Serum by Two-Dimensional Differential Gel Electrophoresis after Depletion of High-Abundant Proteins. *J Proteome Res* 2004;3:1120–7. doi:10.1021/pr049921p.

- [65] Sund J, Alenius H, Vippola M, Savolainen K, Puustinen A. Proteomic Characterization of Engineered Nanomaterial–Protein Interactions in Relation to Surface Reactivity. *ACS Nano* 2011;5:4300–9. doi:10.1021/nn101492k.
- [66] Mao H, Chen W, Laurent S, Thirifays C, Burtea C, Rezaee F, et al. Hard corona composition and cellular toxicities of the graphene sheets. *Colloids Surf B Biointerfaces* 2013;109:212–8. doi:10.1016/j.colsurfb.2013.03.049.
- [67] Gu Z, Yang Z, Chong Y, Ge C, Weber JK, Bell DR, et al. Surface Curvature Relation to Protein Adsorption for Carbon-based Nanomaterials. *Sci Rep* 2015;5. doi:10.1038/srep10886.
- [68] Owens III DE, Peppas NA. Opsonization, biodistribution, and pharmacokinetics of polymeric nanoparticles. *Int J Pharm* 2006;307:93–102. doi:10.1016/j.ijpharm.2005.10.010.
- [69] Ogawara K, Furumoto K, Nagayama S, Minato K, Higaki K, Kai T, et al. Pre-coating with serum albumin reduces receptor-mediated hepatic disposition of polystyrene nanosphere: implications for rational design of nanoparticles. *J Controlled Release* 2004;100:451–5. doi:10.1016/j.jconrel.2004.07.028.
- [70] Peng Q, Zhang S, Yang Q, Zhang T, Wei X-Q, Jiang L, et al. Preformed albumin corona, a protective coating for nanoparticles based drug delivery system. *Biomaterials* 2013;34:8521–30. doi:10.1016/j.biomaterials.2013.07.102.
- [71] Walkey CD, Olsen JB, Song F, Liu R, Guo H, Olsen DWH, et al. Protein Corona Fingerprinting Predicts the Cellular Interaction of Gold and Silver Nanoparticles. *ACS Nano* 2014;8:2439–55. doi:10.1021/nn406018q.
- [72] Rahman M, Laurent S, Tawil N, Yahia L, Mahmoudi M. Nanoparticle and Protein Corona. *Protein-Nanoparticle Interact.*, vol. 15, Berlin, Heidelberg: Springer Berlin Heidelberg; 2013, p. 21–44.
- [73] Lindman S, Lynch I, Thulin E, Nilsson H, Dawson KA, Linse S. Systematic investigation of the thermodynamics of HSA adsorption to N-iso-propylacrylamide/N-tert-butylacrylamide copolymer nanoparticles. Effects of particle size and hydrophobicity. *Nano Lett* 2007;7:914–20.
- [74] Moghimi SM, Andersen AJ, Ahmadvand D, Wibroe PP, Andresen TL, Hunter AC. Material properties in complement activation. *Adv Drug Deliv Rev* 2011;63:1000–7. doi:10.1016/j.addr.2011.06.002.
- [75] Gessner A, Lieske A, Paulke B-R, Müller RH. Functional groups on polystyrene model nanoparticles: Influence on protein adsorption. *J Biomed Mater Res A* 2003;65A:319–26. doi:10.1002/jbm.a.10371.
- [76] Qian ZM, Li H, Sun H, Ho K. Targeted Drug Delivery via the Transferrin Receptor-Mediated Endocytosis Pathway. *Pharmacol Rev* 2002;54:561–87.

[77] Meng F, Ugaz VM. Instantaneous physico-chemical analysis of suspension-based nanomaterials. *Sci Rep* 2015;5. doi:10.1038/srep09896.